12th International Conference on Fracture Mechanics of Concrete and Concrete Structures
FraMCoS-12
B.L.A. Pichler, Ch. Hellmich, P. Preinstorfer (Eds)

https://doi.org/10.21012/FC12.1184
TT-F:3

NON-DESTRUCTIVE DETECTION OF SURFACE DAMAGE IN HOLLOW GRAVITY TYPE OF CONCRETE DAM BY USING PASSIVE INFRARED THERMOGRAPHY DATA WITH DEEP LEARNING METHOD

TETSUYA SUZUKI[*], KAZUMA SHIBANO[†],

TAIKI HAGIWARA[††] AND NINEL ALVER[†††]

[*] Institute of Agriculture, Niigata University, Niigata 950-2181, Japan
e-mail: suzuki@agr.niigata-u.ac.jp

[†] Graduate School of Science and Technology, Niigata University, Niigata 950-2181, Japan
e-mail: kazuma3267@gmail.com

[††] Civil Engineering Research Institute for Cold Region, PWRI, Sapporo City, Hokkaido, Japan
e-mail: t.hagiwara8220@outlook.com

[†††] Department of Civil Engineering, Ege University, Bornova, Izmir 35100, Turkey
e-mail: ninelalver@gmail.com

Key words: Concrete dam, Surface temperature, Heat balance model, Deep learning model, LSTM

Abstract: For large-scale infrastructure, such as concrete dams, a non-destructive and non-contact testing method is essential for estimating subsurface damage. Passive infrared thermography is an effective technique for detecting this type of damage, relying on heat capacity differences within the concrete. Since surface temperature distribution irregularities correlate with crack propagation and material degradation, passive infrared thermography can be applied to assess damage progression in concrete structures. This study investigates the relationship between thermal responses and subsurface damage using a combination of heat balance analysis and deep learning models, contributing to the field of fracture mechanics and structural integrity assessment. In this study, the thermal behavior of a concrete dam is analyzed using heat balance modeling and Long Short-Term Memory (LSTM) to assess subsurface damage. Measured and predicted surface temperatures at exudation and non-damaged points are compared to investigating the correlation between thermal distribution irregularities and exudation. The results indicate that a higher estimation accuracy is achieved by LSTM compared to heat balance analysis, as shadow effects, latent heat transfer and moisture dynamics are implicitly considered—factors affecting surface temperature distribution. Through these analyses, the potential of passive infrared thermography is validated as a non-destructive method for monitoring and assessing structural integrity in large-scale concrete infrastructure.

1 INTRODUCTION

Dams have been a significant role in ensuring a stable supply of water for flood control, irrigation, drinking water, livestock and hydraulic power generation [1]. Most large dams were constructed after the 1950s, and the number of new dam constructions declined around the 1990s, with the exception of South America [2]. The performance of these structures can deteriorate over time due to long-term service, environmental factors, operational loads, and accumulated damage

from extreme events such as earthquakes. Crack propagation, material fatigue and moisture ingress are key factors in the degradation of concrete structures, requiring advanced monitoring techniques for early damage detection. Some countries face challenges in managing aging dams due to inadequate funding [3]. Infrared thermography, combined with numerical modelling and deep learning, provides a powerful approach for evaluating the progression of subsurface damage over time. This study aims to bridge the gap between thermal analysis and fracture mechanics, supporting predictive maintenance strategies for large-scale concrete infrastructure. Elastic wave techniques are commonly used for the inspection of concrete structures as a non-destructive testing method. However, their application to large-scale structures is challenging due to issues related to accessibility and comprehensiveness. Passive infrared thermography is an optimal technique for detecting subsurface defects over a wide area at once [4]. Thermography techniques utilize the heat capacity of materials, and in general, the contrast in surface temperature can indicate subsurface damage in concrete structures. Previous studies have focused on effective time windows for infrared thermography, as the contrast in surface temperature changes over time due to environmental and weather conditions [5]. These efforts have primarily been applied to concrete specimens to investigate the relationship between time and detectability. However, time is not a significant factor affecting surface temperature in the context of in-service concrete structures. The surface temperature of concrete is mainly determined by weather conditions, heat conduction into the concrete, subsurface damage and surface conditions. Therefore, the heat balance of concrete needs to be calculated to estimate subsurface damage accurately.

In this study, the surface temperature of concrete, measured by passive infrared thermography, is verified through heat balance analysis and a deep learning method. The proposed method is applied to an in-service hollow gravity-type concrete dam, where prediction accuracy and surface temperature contrast are compared. The heat balance analysis calculates the surface temperature by considering weather conditions and heat conductivity. Additionally, a deep learning method for sequential data, Long Short-Term Memory (LSTM) [6], is used to implicitly train the relationship between surface temperature and weather data.

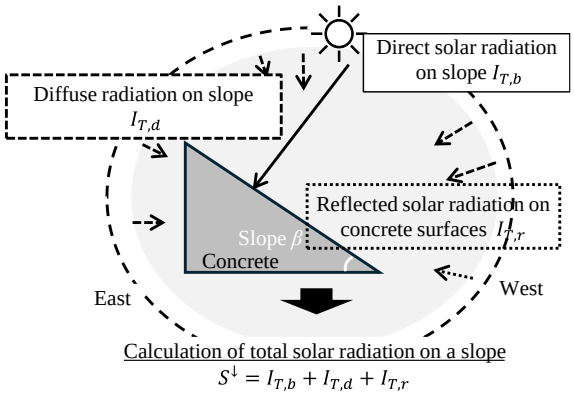

Figure 1: Heat balance analysis.

2 ANALYTICAL PROCEDURES

The surface temperature of concrete is calculated using heat balance analysis and LSTM, with incorporated weather data. To assess the impact of cracking and moisture ingress on heat transfer mechanisms, the correlation between thermal distribution irregularities and structural degradation is analyzed. These methods are calibrated using measured surface temperature data obtained from a thermocouple. The prediction accuracy is evaluated by Mean Absolute Error (MAE), which is a comparison of heat balance analysis and LSTM results.

2.1 Heat balance analysis

The heat balance of the concrete surface is expressed by equation (1).

$$R_n = H + G, \tag{1}$$

where, R_n is the net radiation (W/m^2), H is the sensible heat transfer (positive upward, W/m^2) and G is the ground conduction heat (positive downward, W/m^2).

$$R_n = (1 - ref)S^{\downarrow} - \epsilon\left(\sigma {T_S}^4 - L^{\downarrow}\right), \quad (2)$$

where, ref is the albedo, $S^{\downarrow}$ is the total solar radiation on the slope (W/m^2), ϵ is the emissivity (black body degree), T_S is the concrete surface temperature (K), σ is the Stefan-Boltzmann constant (5.67×10^{-8} W/(m^2 ・K^4)), and $L^{\downarrow}$ is the longwave radiation from the atmosphere that does not include solar radiation (W/m^2). The albedo is the ratio of the reflected light flux to the incident light flux when radiation is incident on an object. In this study, the latent heat transfer is ignored, therefore, the effect of rainfall is not assumed. The surface temperature is calculated assuming that weather conditions, concrete surface parameters (albedo and emissivity) and thermal properties (specific heat, density and thermal conductivity of concrete and air) are known. The sensible heat transfer H is shown in equation (3).

$$H = c_a \rho_a C_H U (T_S - T_a), \quad (3)$$

where, c_a is the specific heat at constant pressure of air (J/(K・kg)), ρ_a is the density of air (kg/m^3), $C_H U$ is the exchange rate of sensible heat transfer and T_a is the air temperature. The exchange rate varies depending on the type of surface , difference in roughness, the surface is treated as bare ground and the following equation is used in this study,

$$C_H U = 0.0027 + 0.0031U. \quad (4)$$

The heat conduction differential equation for the internal temperature T_G of concrete is shown in the following equation.

$$\frac{\partial T_G}{\partial t} = \frac{\lambda_c}{c_c \rho_c} \frac{\partial^2 T_G}{\partial z^2}, \quad (5)$$

where, λ_c is the thermal conductivity of concrete (W/(m・K)), c_c is the specific heat at constant pressure of concrete (J/(K・kg)), ρ_c is the density of concrete (kg/m^3), t is time (s), and z is depth (m).

The conduction heat $G(z)$ in concrete at depth z from the surface is expressed by the following equation,

$$G(z) = \lambda_c \frac{dT_G}{dz}. \quad (6)$$

On the other hand, by integrating the equation obtained by rewriting equation (5):

$$\frac{\partial G(z)}{\partial z} = -\frac{d}{dt}(c_c \rho_c T_G). \quad (7)$$

By integrating this, the conductive heat G at the concrete surface is obtained.

$$G \equiv G_{(z=0)} = \int_0^D \frac{d(c_c \rho_c T_G)}{dt} dz, \quad (8)$$

where, D is the depth (m) at which thermal conduction becomes zero. In this study, D is set to 1.0 m, which is the depth of actual embankment and the point where $z = D$ is considered to be the deepest point in the heat balance analysis.

To calculate the total solar radiation on the slope, the total solar radiation on the horizontal surface is separated into direct solar radiation on the horizontal surface that reaches the concrete surface directly from the sun and diffuse solar radiation on the horizontal surface (direct and diffuse separation), and then the solar radiation on the slope (direct solar radiation on the slope, diffuse solar radiation on the slope and reflected solar radiation on the concrete surface) is calculated taking into account the inclination of the structure. Diffuse solar radiation is solar radiation that is scattered by particles in the atmosphere as it passes through the Earth's atmosphere and reaches the earth's surface from the entire sky.

The direct and diffuse separation is shown in the following equation.

$$I_G = I_b + I_d, \quad (9)$$

where, I_G is the total solar radiation on the horizontal surface (W/m^2), I_b is the direct solar radiation on the horizontal surface (W/m^2) and I_d is the diffuse solar radiation on the horizontal surface (W/m^2).

Conversion from horizontal direct solar radiation to inclined direct solar radiation is calculated by following equation.

$$I_{T,b} = I_b \cos i, \quad (10)$$

where, $I_{T,b}$ is the amount of direct solar radiation on the slope (W/m^2) and i is the angle of incidence of direct solar radiation. The conversion coefficient for direct solar radiation on a horizontal surface to inclined direct solar radiation is shown in the following equation based on the relationship between the sun's position and the slope.

$$\cos i = \cos\beta \sin h + \sin\beta \cos h \cos(A_S - A_W), \quad (11)$$

where, β is the inclination angle of the slope relative to the horizontal surface, h is the solar altitude, A_S is the solar azimuth angle and A_W is the azimuth angle of the slope.

The Erbs model is used to separate the direct and diffuse solar radiation [7].

$$I_{T,d} = I_d F, \quad (12)$$

where, $I_{T,d}$ is the amount of inclined diffuse solar radiation (W/m^2) and F is a function that expresses the proportion of inclined diffuse solar radiation to the horizontal diffuse solar radiation.

The amount of reflected solar radiation on the concrete surface is calculated using a uniform distribution model that assumes that the radiance distribution of the sky is uniform.

$$I_{T,r} = I_G \frac{1 - \cos\beta}{2} ref, \quad (13)$$

where, $I_{T,r}$is the reflected solar radiation on the concrete surface (W/m^2).

The total solar radiation on the slope is calculated using equations (10), (12), and (13).

$$S^{\downarrow} = I_{T,b} + I_{T,d} + I_{T,r}. \quad (14)$$

2.2 Long Short-Term Memory (LSTM)

To estimate the concrete surface temperature based on meteorological data, LSTM is applied. LSTM, a variant of the recurrent neural network (RNN) developed for sequential data, is capable of learning long-term dependencies and is widely used. Although many variants of LSTM have been proposed, none have been shown to significantly outperform simple LSTM architecture. Therefore, the model proposed by Hochreiter and Schmidhuber (1997) is adopted [6].

For prediction using LSTM, data from July 2023 to May 2024, is used as training and validation data, while data from June 2024 to October 2024, is used as test data. The meteorological data used to predict surface temperature consists of 11 items: solar radiation, precipitation, relative humidity, air temperature, barometric pressure, wind speed, wind gust, wind direction, lightning strikes, average lightning distance and downward longwave radiation. The adjusted hyperparameters are window size, batch size, hidden size, number of layers and epoch. The window size represents the length of the input sequence. Hidden size indicates the dimensionality of the hidden states. Larger values enable the learning of more complex patterns but increase computational costs. Num layers indicates the number of LSTM layers, adjusting the model's expressive capacity. Epoch specifies the number of iterations the dataset passes through during training. While increasing the number of epochs improves the fit to the training data, exceeding an appropriate value risks overfitting. Hyperparameter tuning is performed manually to explore the combination that minimizes error.

3 MEASUREMENT PROCEDURE

A series of measurements were conducted at a hollow gravity-type concrete dam. The surface temperature of the concrete was measured using a thermocouple and passive infrared thermography as continuous observations. Meteorological data were recorded for the same period.

3.1 Measurement structure

The measurement structure is a hollow gravity-type concrete dam, as shown in Figure 2. This dam was constructed in 1974. No surface damage is evident, however, damage resulting from freeze-thaw cycles is observed in part of the structural concrete. Exudation is visible on the embankment surface on the left side, as shown in Figure 3. The concrete surface of interest in this study is the embankment of the dam structure, which faces downstream. The surface temperature, measured using a thermocouple, was recorded

at a point on the embankment on the right side of the bank (refer to "Thermocouple" in Figure 2). The area of interest for infrared thermography encompasses the embankment surface from the center to the left side of the bank.

3.2 Measurement of surface temperature

A K-type thermocouple was attached to the concrete surface, with the junction adhered using a cement-based adhesive. Temperature data were recorded at 10-minute intervals and logged by a data logger.

3.3 Passive infrared thermography

Passive infrared thermography measurements were conducted using a thermal camera (Zenmuse XT2, FLIR) mounted on a UAV (Matrice 210, DJI). The measurement interval was set to 1 hour, with measurements taken between 9 a.m. and 4 p.m., once per month.

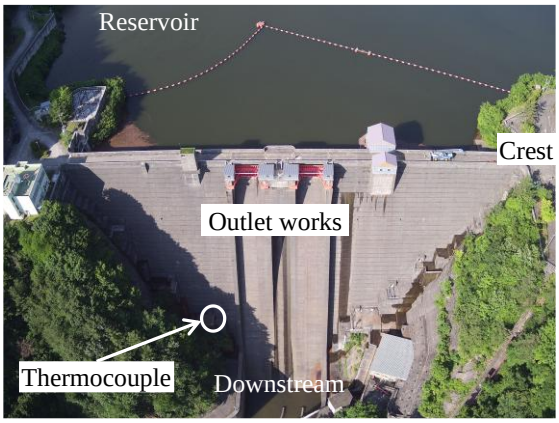

Figure 2: Hollow gravity-type of concrete dam.

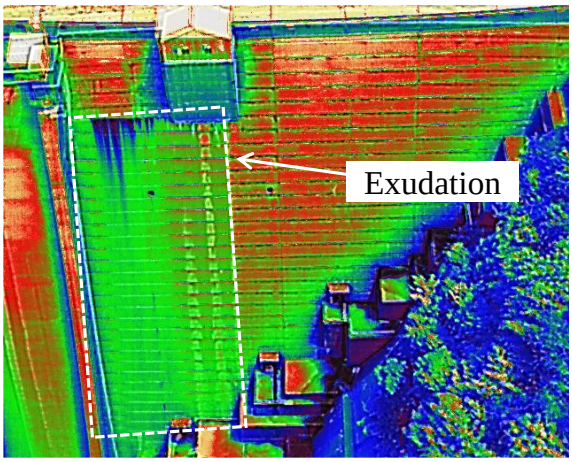

Figure 3: Exudation on the left side embankment.

3.4 Meteorological measurements

Weather data were recorded by an ATMOS-41 Weather Station (METER). The weather data items included solar radiation, precipitation, relative humidity, air temperature, barometric pressure, wind speed, wind gust, wind direction, lightning strikes, average lightning distance and downward longwave radiation. The measurement interval was set to 10 minutes. The weather station was installed at the crest of the dam.

4 RESULTS AND DISCUSSION

4.1 Meteorological conditions surrounding concrete dam

The sequential changes in surface temperature, measured by the thermocouple and meteorological data are shown in Figure 4. The horizontal axis index indicates the measurement points at 10-minute intervals. The trends in surface temperature, solar radiation, precipitation, wind speed and air temperature exhibit a seasonal pattern with peaks and troughs occurring each year. The global trends in surface and air temperature are closely matched, with the surface temperature consistently higher than the air temperature. Solar radiation increases gradually, with fluctuations corresponding to changes in both surface and air temperature. While the seasonal variation in precipitation is unclear, the likelihood of substantial rainfall is low. The change in wind speed tends to be inversely correlated with the other parameters.

4.2 Calculation of surface temperature by heat balance analysis and LSTM

The thermal properties of concrete are calibrated using a grid search within the range of reference values for heat balance analysis. The calibrated values for density, specific heat, conductivity, emissivity, and albedo of concrete are 2,400 kg/m³, 1,260 J/kgK, 1.4 W/mK, 0.96, and 0.4, respectively. The prediction results of surface temperature, obtained through both heat balance analysis and LSTM, are shown in

Figures 5 and 6. The mean absolute error (MAE) between measured and calculated values is presented in Table 1. The MAE for heat balance analysis and LSTM are 2.3 and 1.3°C, respectively. The MAE for the training, evaluation, and test data in LSTM are 1.2°C, 2.1°C and 1.1°C, respectively. The MAE for heat balance analysis is higher than that for LSTM. In most cases, the calculated values from the heat balance analysis are higher than the measured values from the thermocouple. The surface temperature calculated by heat balance analysis follows the peak of the daily change. However, the surface temperature calculated by LSTM does not reach the peak of daily changes. Both heat balance analysis and LSTM are capable of reproducing the overall trend of surface temperature. These results suggest that LSTM effectively learns the features of surface temperature using 11 meteorological data items and can reproduce the measured surface temperature of concrete. In this study, solar radiation, wind speed, downward longwave radiation and air temperature are considered in the heat balance analysis. Shadow effects are observed on the actual concrete surface, as the dam embankment faces west and shadowing by trees is apparent in the evening. However, shadow effects and latent heat transfer are not considered in the analysis, which results in lower accuracy in the reproduction of surface temperature. Deep learning methods for time-series data are effective for estimating concrete surface temperature using weather data. In contrast, heat balance analysis that incorporates shadow effects and latent heat transfer has the potential to more accurately estimate concrete surface temperature.

4.3 Validation of passive infrared thermography by heat balance analysis and LSTM

The comparison between the measured concrete surface temperature by passive infrared thermography and the calculated values by heat balance analysis and LSTM is shown in Figure 7. Missing data points are indicated by the cancellation of flights due to

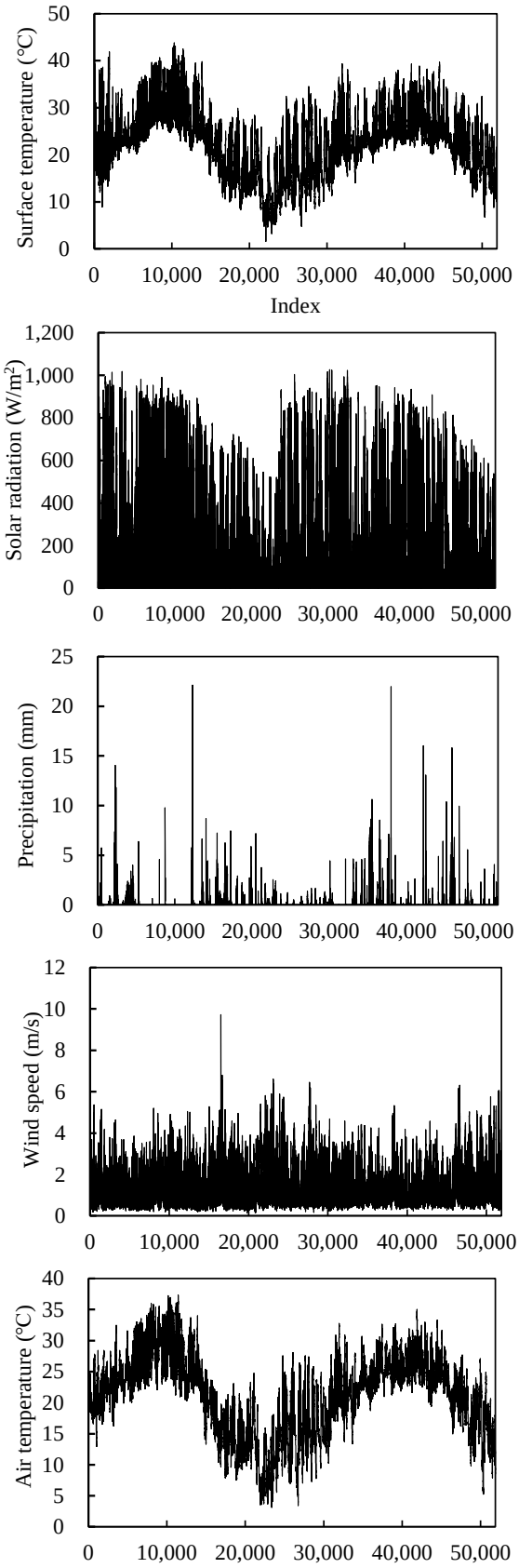

Figure 4: Sequential change of surface temperature by the thermocouple and meteorological data

rainfall for samples No. 7, 8, 9, and 12. The surface temperature at the exudation point, measured by the infrared camera, is lower than that of the non-damaged point during the periods of No. 1 and No. 9. For most other periods, the surface temperature at the exudation point is higher than at the non-damaged point. The extraction point for surface temperature from the infrared image is located on the left side of the embankment, while the thermocouple is set on the lower right side. When water is not trickling from the exudation point, the surface temperature at the exudation point is typically higher than at the non-damaged point. As discussed in section 4.2, the prediction accuracy by heat balance analysis is lower than that of LSTM. The surface temperature trend for sample No. 1, where exudation phenomena are confirmed, is shown in Figure 7(b). The calculated surface temperature by LSTM closely matches the measured surface temperature at the non-damaged point, as recorded by both the thermocouple and the infrared camera. The

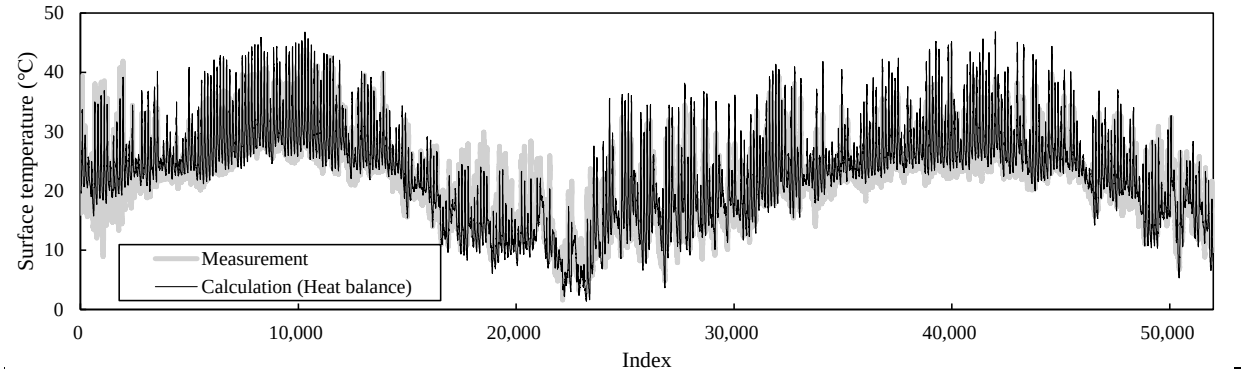

Figure 5: Calculation result of concrete surface temperature by heat balance analysis.

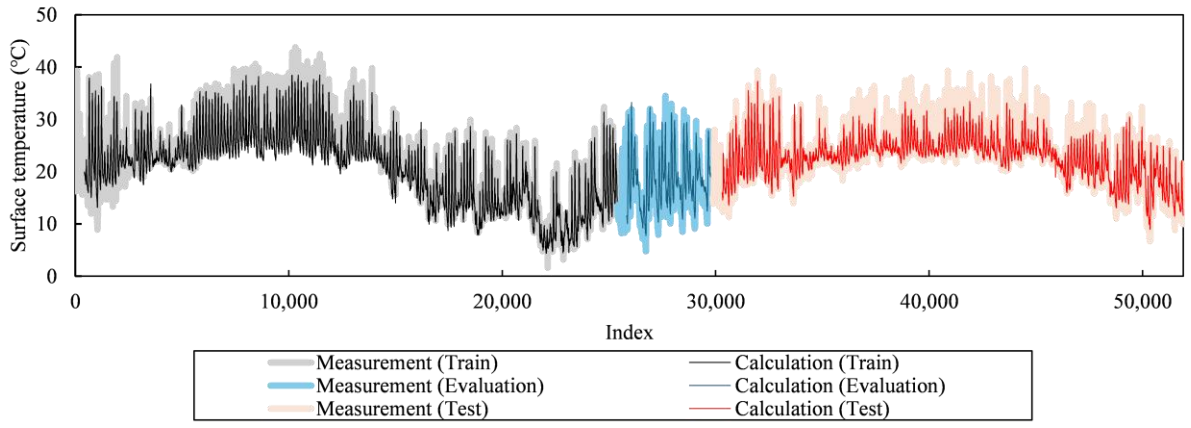

Figure 6: Calculation result of concrete surface temperature by LSTM.

Table 1: Mean Absolute Error (MAE) between measured surface temperature by the thermocouple and calculated value by heat balance analysis and LSTM

	Heat balance analysis	LSTM
MAE (°C)	2.3	1.3 (Train: 1.2, Evaluation: 2.1, Test: 1.1)

relationship between the difference in surface temperature between the exudation point and the non-damaged point, and the estimated accuracy of both methods, is presented using the mean absolute error (MAE) in Table 2. The MAE between the surface temperature at the exudation and non-damaged points is 8.0°C. The MAE between the measured surface temperature from the infrared camera and the calculated surface temperature by heat balance analysis and LSTM are 5.6°C and 3.5°C, respectively. The prediction accuracy of both methods is sufficient to distinguish surface temperature changes between the non-damaged and exudation points. These results confirm that both heat balance analysis and LSTM are effective in reproducing concrete surface temperature and validating passive infrared thermography. Prediction accuracy by LSTM is higher than heat balance analysis since shadow effects and latent heat transfer, which are not included in the heat balance analysis, are considered by LSTM. This suggests that complex relationships between environmental factors and material degradation can be implicitly learned by deep learning-based models. The results demonstrate that surface temperature variations detected via passive

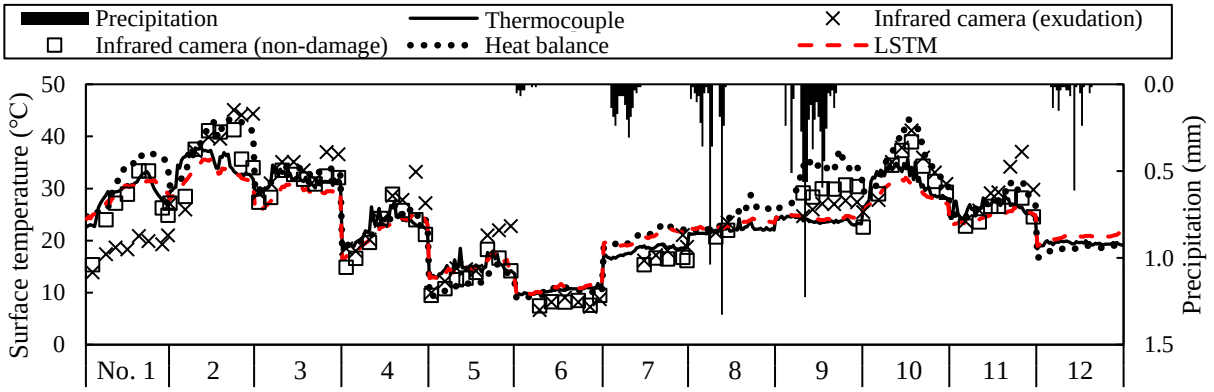

(a) For two years period except for winter season

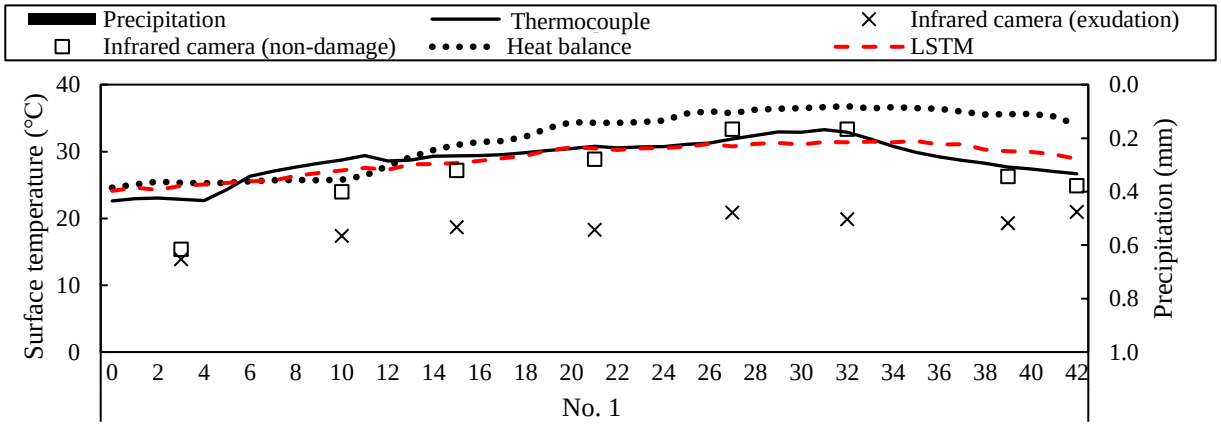

(b) Zoom up for period of No. 1

Figure 7: The comparison of measured surface temperature by passive infrared thermography and calculation value by heat balance analysis and LSTM.

Table 2: MAE between the surface temperature of exudation and non-damaged part, and measured surface temperature by infrared camera and calculation value by heat balance analysis and LSTM for period of No. 1

	Exudation-Non damaged	Heat balance analysis	LSTM
MAE (°C)	8.0	5.6	3.5

infrared thermography can serve as an indicator of crack formation and internal damage, consistent with the principles of fracture mechanics.

5 CONCLUSIONS

A reliable framework for predicting concrete surface temperature and validating passive infrared thermography is provided by the heat balance analysis and LSTM. This study contributes to the field of fractured mechanics by demonstrating that irregularities in thermal distribution can be associated with damage progression in concrete structures. The findings support the integration of passive infrared thermography-based monitoring with numerical simulations for long-term structural assessments, which enhances predictive maintenance strategies for aging infrastructure. While LSTM offers higher accuracy and flexibility, heat balance analysis retains value for understanding thermal properties and physical phenomena. Future advancements, such as incorporating shadow effects and latent heat transfer into heat balance analysis, could further improve prediction accuracy. With validation from these methods, passive infrared thermography proves to be a reliable tool for monitoring surface temperature and detecting damage in concrete structures.

REFERENCES

[1] International Commission on large dams, General Synthesis, 2024.

[2] Zhang, A. T. and Gu, V. X., 2023. Global Dam Tracker: A database of more than 35,000 dams with location, catchment, and attribute information. *Scientific data*, **10**(1), 111.

[3] Ho, M., Lall, U., Allaire, M., Devineni, N., Kwon, H. H., Pal, I., Raff, D. and Wegner, D., 2017. The future role of dams in the United States of America, *Water Resources Research*, **53**(2), 982-998.

[4] Pozzer, S., Omidi, Z., El Refai, A., López, F., Ibarra-Castanedo, C. and Maldague, X., 2024. Passive infrared thermography for subsurface delamination detection in concrete infrastructure: Capabilities, *Construction and Building Materials*, **419**, 135542.

[5] Hiasa, S., Birgul, R., Matsumoto, M., and Catbas, F. N., 2018. Experimental and numerical studies for suitable infrared thermography implementation on concrete bridge decks, *Measurement*, **121**, 144-159.

[6] S. Hochreiter and J. Schmidhuber, 1997. Long short-term memory, *Neural Comput.*, **9**(8), 1735–1780

[7] Erbs, D. G., Klein, S. A. and Duffie, J. A., 1982. Estimation of the Diffuse Radiation Fraction for Hourly, Daily and Monthly-Average Global Radiation, *Solar Energy*, **28**(4), 293–302.